Carcinogenesis vol.35 no.2 pp.373–382, 2014
doi:10.1093/carcin/bgt380
Advance Access publication November 26, 2013

Anti-YKL-40 antibody and ionizing irradiation synergistically inhibit tumor vascularization and malignancy in glioblastoma

Rong Shao[1,2,*], Ralph Francescone[2], Nipaporn Ngernyuang[3], Brooke Bentley[4], Sherry L.Taylor[5], Luis Moral[4] and Wei Yan[1]

[1]Department of Veterinary and Animal Sciences and [2]Molecular and Cellular Biology Program, Morrill Science Center, University of Massachusetts, Amherst, MA 01003, USA, [3]Faculty of Associated Medical Sciences, Khon Kaen University, Khon Kaen 40002, Thailand and [4]Department of Pathology and [5]Division of Neurosurgery, Baystate Medical Center, Tufts University, Springfield, MA 01199, USA

*To whom correspondence should be addressed. Tel: +1 (413) 794 9568; Fax: +1 (413) 794 0857;
Email: rshao@vasci.umass.edu

Chemo/radiotherapies are the most common adjuvant modality treated for patients with glioblastoma (GBM) following surgery. However, the overall therapeutic benefits are still uncertain, as the mortality remains high. Elevated expression of YKL-40 in GBM was correlated with increases in mural cell-associated vessel coverage, stability and density, and decreases in vessel permeability and disease survival. To explore the potential role of YKL-40 in mural cell-mediated tumor vascularization, we employed an anti-YKL-40 neutralizing antibody (mAY) and ionizing irradiation (IR) in xenografted brain tumor models. Although single treatment with mAY or IR partially increased mouse survival, their combination led to dramatic inhibition in tumor growth and increases in mouse survival. mAY blocked mural cell-mediated vascular stability, integrity and angiogenesis; whereas IR merely promoted tumor cell and vascular cell apoptosis. Vascular radioresistance is at least partially attributed to expression of YKL-40 in mural cells. These divergent effects were also recapitulated in cultured systems using endothelial cells and mural cells differentiated from glioblastoma stem-like cells (GSCs). Dysfunction of intercellular contact N-cadherin was found to mediate mAY-inhibited vascularization. Collectively, the data suggest that the conjunction therapy with mAY and IR synergistically inhibit tumor vascularization and progression. The evidence may shed light on a new adjuvant therapy in clinic.

Introduction

Glioblastoma (GBM), the most lethal primary brain tumor, exhibits the poorest prognosis of all brain tumors with a median survival of around 12–15 months (1). GBM is characterized by strong vascular proliferation that is associated with tumor cell growth, invasion, resistance to chemo/radiotherapy and short survival. Although GBMs rarely spread outside the nervous system, they present as infiltrating tumors with invasion into cranial brain tissue, thus preventing curative surgical removal. Regardless of extensive surgical excision and postoperative adjuvant radio/chemotherapy, <3% of cancer patients can survive >5 years and approximately half of patients recur and progress (2). Currently, most of anti-GBM chemotherapies primarily focus on eliminating rapidly proliferating cancer cells but fail to target a rare and radioresistant fraction of tumor cells known as GBM stem-like cells (GSCs) (3,4). GSCs express neural stem cell markers CD133 and Nestin and retain stem cell properties including self-renewal and differentiation into neural lineages including neurons, astrocytes and oligodendrocytes (5). Following radiotherapy and chemotherapy, a small population of GSCs is unexpectedly enriched to constitute a significant portion of the overall tumor mass and also support tumor regrowth by reinitiating vascular microcirculation (6–8). GSCs were recently found to be capable of transdifferentiation into a large population of vascular mural cells or pericytes and a small population of endothelial cells, both of which participate in tumor vascularization (9–12).

YKL-40 is a 40 kDa secreted glycoprotein discovered as a heparin-binding protein and belongs to the chitinase gene family that binds to chitin-like oligosaccharides (13). However, it does not have chitinase/hydrolase activity because of the substitution of an essential glutamic acid with leucine in the chitinase-3-like catalytic domain (13). YKL-40 is normally expressed by a number of different cell types including chondrocytes (14), synoviocytes (15), vascular smooth muscle cells (16), macrophages (17) and neutrophils (18), and it has been recognized as a growth factor capable of stimulating connective tissue cell growth and endothelial cell migration and inhibiting mammary epithelial cell differentiation (19,20). However, the pathophysiological function of YKL-40 remains to be fully determined.

A putative role of YKL-40 in cancer progression has emerged for more than a decade. YKL-40 is one of the top upregulated genes found in GBM by the differential gene expression profiling including Serial Analysis of Gene Expression (SAGE) and microarray databases (21,22). A wealth of clinical evidence has revealed that high serum levels of YKL-40 and tumor protein or transcript levels of YKL-40 are correlated with cancer invasiveness, radioresistance, recurrence and short survival of patients with GBM (21–27). We have found that YKL-40 acts as an angiogenic factor to induce tumor angiogenesis and the molecular mechanism is associated with activation of membrane protein syndecan-1 through its interaction with heparan sulfate chains present at the ectodomain of syndecan-1 on cell surface (28–30). Elevated YKL-40 in GBM is associated with tumor angiogenesis and radioresistance, which may at least partially contribute to the tumor malignancy (29,30). In concert with our findings, radiotherapy-resistant GBMs expressed elevated levels of YKL-40 (23,31). Collectively, these data suggest that YKL-40 mediates tumor radioresistance and recurrence, and that serum levels of YKL-40 may serve as a diagnostic and prognostic biomarker.

Tumor angiogenesis is typically characterized by neovascular tubule formation of endothelial cells followed by abluminal recruitment of mural cells, the vessel-supporting cells (32). Spatial coordination and regulation of cell–cell tight contacts commit endothelial cells and mural cells to orchestrate the vessel wall, which offers adequate blood perfusion and the delivery of nutrients and oxygen for tissue proliferation (33). Recently, we have uncovered a new angiogenic role of YKL-40 in tumor vascular wall integrity characterized by the intimate interaction between endothelial cells and mural cells (34). A neutralizing monoclonal anti-YKL-40 antibody (mAY) created from our lab demonstrates the ability to block angiogenesis in xenografted tumors (35). However, it is poorly understood if ionizing irradiation (IR) has the same ability as mAY to inhibit angiogenesis, if mAY- and/or IR-inhibited tumor angiogenesis is through impairing mural cell activity and/or endothelial cell activity, and if so, what are molecular bases underlying this inhibition. In light of future development of efficacious therapy for patients with GBM, it is imperative to develop and evaluate novel strategies of single and conjunction therapy with mAY and IR in preclinical trials using animal brain tumor models.

Abbreviations: Calcein AM, calcein acetoxymethyl; DAPI, 4′,6-diamidino-2-phenylindole; FBS, fetal bovine serum; FITC, fluorescein isothiocyanate; GBM, glioblastoma; GSC, glioblastoma stem-like cell; GSC-DC, GSC-differentiated cell; HMVEC, human microvascular endothelial cell; IHC, immunohistochemistry; IR, ionizing irradiation; SMa, smooth muscle alpha actin.

Materials and methods

GSCs and GSC-differentiated cells

GSCs were isolated from tumor samples of patients with GBM following approval of Baystate Medical Center Institutional Review Board (9). These GSCs were propagated in stem cell medium Dulbecco's modified Eagle

medium/F12 supplemented with B27 (Invitrogen, Carlsbad, CA) and 20 ng/ml basic fibroblast growth factor and epidermal growth factor. For all the experiments in cultured condition *in vitro*, GSCs were differentiated into mural-like cells (GSC-DCs) in the presence of Dulbecco's modified Eagle medium containing 10% fetal bovine serum (FBS) for 1 week (9). During this differentiation, the cells were exposed to 10 Gy IR from a radioactive cesium source two times in presence of mAY (10 µg/ml) or mIgG (10 µg/ml) as a control. Human microvascular endothelial cells (HMVECs) were grown in EBM-2 (Lonza, Allendale, NJ) supplemented with 5 µg/ml hydrocortisone, 10 ng/ml human epidermal growth factor, 10% FBS and penicillin/streptomycin.

Immunoprecipitation and immunoblotting

Cell lysate samples were processed as described previously (34). Samples were subjected to running sodium dodecyl sulfate–polyacrylamide gel electrophoresis and polyvinylidene fluoride membranes were incubated with one of a series of primary antibodies against N-cadherin (Invitrogen), β-catenin, syndecan-1 (Santa Cruz Biotechnology, Santa Cruz, CA), YKL-40 (our lab), caspase-3 (Enzo Life Science, Farmingdale, NY), smooth muscle alpha actin (SMa) (Abcam, Cambridge, MA) and actin (Sigma, St Louis, MO). Membranes were then incubated with goat anti-mouse or anti-rabbit secondary antibodies (Jackson Lab, Bar Harbor, ME). Specific signals were detected by enhanced chemiluminescence (VWR, Rockford, IL). For immunoprecipitation, cell lysates were incubated with an anti-N-cadherin antibody at 4°C overnight followed by incubation with protein G Sepharose 4 Fast Flow beads at 4°C for 4 h. The immunocomplex was extensively washed and the samples were run for immunoblotting against β-catenin or syndecan-1.

Cell permeability

HMVECs or GSC-DCs (2×10^5 cells) were loaded onto 0.4 µm 24 Transwells precoated with 100 µg/ml collagen IV overnight. For cell coculture, GSC-DCs (1×10^5 cells) were loaded for 2 h prior to HMVECs (1×10^5 cells). Twenty-four hours later, Dextran conjugated with fluorescein isothiocyanate (FITC) (0.02 mg/ml; Invitrogen) was added on the top of the wells for 4 h. An aliquot from the bottom of the wells was measured for absorbance at 485 nm.

IR of cells and Live/Dead Assay

GSCs were exposed to 0–10 Gy IR. To assay cell viability, Live/Dead mixture with calcein acetoxymethyl (calcein AM) and ethidium homodimer (Invitrogen) was employed, which assessed the number of live and dead cells, respectively. Fluorescent images of live (green) and dead (red) cells were analyzed. The percentages of live and dead cells were quantified.

Immunocytochemistry

The method was described previously (34). Briefly, cells were grown to subconfluence and fixed with 4% paraformaldehyde for 5 min. After permeabilization with Triton 100X, the cells were incubated with an anti-N-cadherin monoclonal antibody (1:100; Invitrogen) at 4°C overnight followed by incubation with a secondary anti-mouse Alexa Fluor 488 (1:1000; Invitrogen) for 2 h. Then, the samples were incubated with a polyclonal anti-β-catenin (1:100; Santa Cruz) followed by an anti-rabbit Alexa Fluor 555 antibody. Cell nuclei were stained with 4′,6-diamidino-2-phenylindole (DAPI; Invitrogen).

Tube formation assays

HMVEC (2×10^4 cells) were transferred onto 96-well Matrigel (Becton Dickson Lab, Bedford, MA). After 24 h of incubation, tube-forming structures were analyzed.

Stability of vascular tubules

HMVECs (2×10^4 cells) and GSC-DCs (2×10^3 cells) prelabeled with Calcein AM and Calcein Red (5 µg/ml; Invitrogen), respectively, were mixed and loaded onto 96-well Matrigel over 24 h. Tubules with fluorescence were imaged and quantified.

Apoptosis

Cell apoptosis in tumor specimens was detected using a TACS.XL DAB *in situ* apoptosis detection kit (Trevigen, Gaithersburg, MD). In brief, brominated nucleotide (BrdU) was incorporated *in situ* onto the free 3′ OH ends of nuclear DNA fragmentation of apoptotic cells by a terminal deoxynucleotidyl transferase enzyme (TdT). The incorporated BrdU was recognized by a highly specific biotinylated anti-BrdU antibody followed by incubation with streptavidin–horse radish peroxidase solution. Then, the final signal was detected by 3,3′-diaminobenzidine solution. Methyl green was used for counterstaining.

Tumor xenografts in mice

All animal experiments were performed under the approval of Institutional Animal Care and Use Committee of the University of Massachusetts. GSCs (1.5×10^5) in 5 µl of phosphate-buffered saline were injected into right striatum of SCID/Beige mice. Mice were killed when mice displayed decreased locomotion.

Immunohistochemistry and immunofluorescence

Tumor specimens were obtained from patients with GBM. Paraffin-embedded or frozen tumor tissue were cut to 6 µm thickness and processed for immunohistochemical analysis (9). Antibodies included mouse anti-hCD31 (1:100) and SMa (1:500; Dako) antibodies, rat an anti-mCD31 (1:100; BD Bioscience) antibody or rabbit anti-YKL-40 (1:200) and fibrinogen (1:100; Dako) antibodies. In brief, samples were incubated with 3% H_2O_2 for 30 min to block endogenous peroxidase activity, followed by incubation with blocking buffer containing 10% goat serum for 1 h. The samples then were incubated at room temperature for 2 h with one antibody. A secondary antibody against individual primary antibodies conjugated to horse radish peroxidase was added for 1 h. Finally, DAB substrate (Dako) was introduced for several minutes and after washing, methyl green was used for counterstaining. Dual immunohistochemistry (IHC) labeling was performed using a sequential process of one antibody staining followed by another staining. For dual immunofluorescent staining, tumor specimens were incubated with a primary antibody for 2 h followed by incubation with a goat Alexa Fluor 488 or 555 secondary antibody (1:250; Invitrogen) for 1 h. Then the samples were similarly incubated with another primary antibody followed by incubation with a goat Alexa Fluor 555 or 488 secondary antibody for 1 h. Finally, DAPI was added to stain nucleus. NIH ImageJ software was used to quantify vessel density in the single staining of CD31.

Evaluation of YKL-40 levels

A staining density assay was used to classify YKL-40 high (YKL-H) and YKL-40 low (YKL-L) groups, as positive staining ≥30% of tumor density was designated for YKL-H and <30% for YKL-L.

Statistics

Data are expressed as mean ± standard error and n refers to the numbers of individual experiments performed. Differences among groups were determined using one-way analysis of variance analysis followed by the Newman–Keuls test. For two group analysis, a Student's t-test was used. The 0.05 level of probability was used as the criterion of significance.

Results

To evaluate YKL-40 expression in tumors of patients with GBM, we surveyed 10 cases of GBM and analyzed expression levels of YKL-40. Based on the extent of YKL-40 expression in tumors, these 10 samples were assigned into two subsets in which one group ($n = 5$) expressed a higher level of YKL-40 (YKL-H) and the other ($n = 5$) displayed lower expression of YKL-40 (YKL-L) (Figure 1A; Supplementary Table 1, available at *Carcinogenesis* Online). YKL-H demonstrated patient survival ~12 months shorter than did YKL-L, as the mean patient survival in YKL-H was 4.8 months relative to 16.3 months in YKL-L (Figure 1B), suggesting that elevated expression of YKL-40 is associated with poorer prognosis. While almost all of the patients were treated with radiation therapy, 4 of 10 cases also received an anti-vascular endothelial growth factor drug bevacizumab (Avastin) (Supplementary Table 1, available at *Carcinogenesis* Online). It was striking that an average of patient survival after the dual radiation and angiogenic therapies (25.7 months) was 21.7 months longer than single treatment (4.0 months). The data imply that combination therapy with IR and antiangiogenic drugs may improve survival and benefit patients in this small set of tumor samples.

In YKL-H, YKL-40 was strongly expressed by the cells surrounding blood vessels, whereas weaker expression of YKL-40 was located in the bulk of tumor cells; but this expression pattern was not identified in YKL-L (Figure 1A). In an analysis of the association of YKL-40 expression with tumor vascularization, IHC staining with an antibody against CD31, an endothelial cell marker, showed that the vessel density of YKL-H was 2.5-fold higher than that of YKL-L (Figure 1A and C). In addition, most of these vessels in the YKL-H exhibited more visible and larger lumens than the vessels in the YKL-L where vessel lumens collapsed, as 2.4-fold greater vessel diameter in the YKL-H was observed than that in the YKL-L (Figure 1A and C). These data suggest that tumor expression of YKL-40 may be associated with vessel stability and angiogenesis.

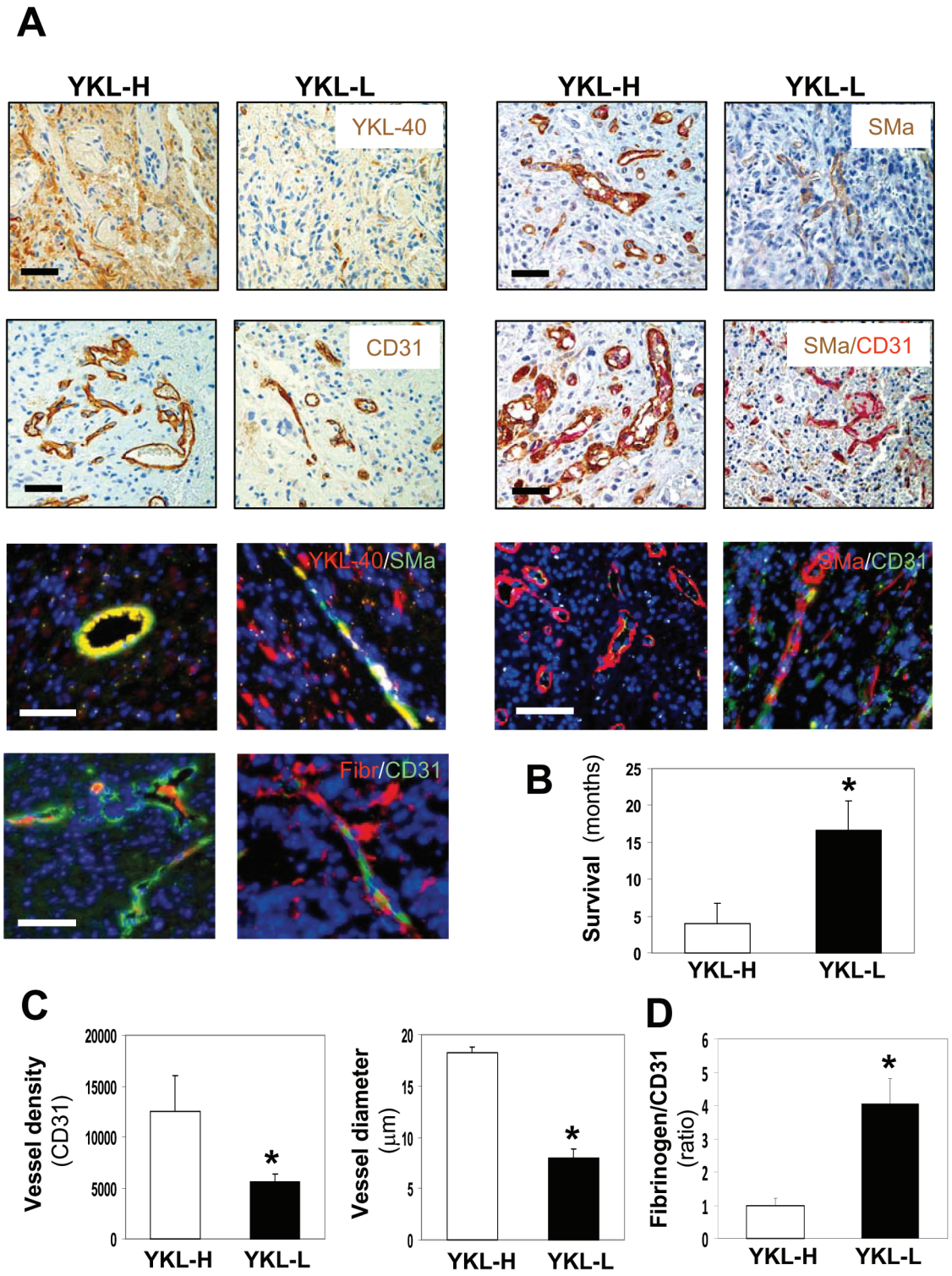

Fig. 1. Elevated expression of YKL-40 in GBM is associated with increased tumor angiogenesis, high vessel stability and decreased survival. (**A**) Ten cases of GBMs were classified into high YKL-40 (YKL-H) and low YKL-40 (YKL-L) groups ($n = 5$ for each). Representative images from each group indicated single staining (brown) of IHC for YKL-40, CD31 and SMa and double staining for SMa (brown) and CD31 (pink). Dual immunofluorescent analyses of YKL-40 (red)/SMa (green), SMa (red)/CD31 (green) and fibrinogen (Red)/CD31 (green) were shown. Yellow images indicated overlay of red and green fluorescence. DAPI (blue) was used to stain the nuclei. Bars: 100 μm. (**B**) Survival data were analyzed in these two groups. *P <0.05 compared with YKL-H, $n = 5$. (**C**) Quantification of CD31 vessel density and vessel diameter from single immunohistochemical staining of CD31 in A. (**D**) Quantification of the ratio of fibrinogen versus CD31 from A for vessel leakage, in which the ratio of fibrinogen density to CD31 density in the YKL-H was set as 1 unit.

It is noted that vessel stability and blood perfusion are dependent on functioning of abluminal vessel-supporting mural cells, another large population of vascular cells covering endothelial cells (32). To test a potential role of YKL-40 in mural cell-mediated vessel stability and integrity, we stained these tumor samples for expression of SMa, a mural cell marker. In concert with vessel staining of CD31, vessel density recognized by SMa in YKL-H was higher than that in YKL-L (Figure 1A). Costaining of CD31 and SMa demonstrated that

the majority of endothelial cell vessels was covered and supported by mural cells in the YKL-H; in contrast, a large portion of CD31-positive vessels in the YKL-L lacked mural cell coverage, indicating vessel collapse. In order to determine if mural cells express YKL-40, we employed a co-immunofluorescent staining approach and found that these vascular mural cells coexpressed SMa and YKL-40 but not CD31 (Figure 1A). In light of the intimate association between vessel stability and perfusion, vascular permeability was measured by diffusion of fibrinogen. Fibrinogen was limited within capillaries in the YKL-H, contrary to that in the YKL-L, which contained more than 4-fold greater diffusion of fibrinogen out of vessels, indicating leakier vasculature (Figure 1A and D). These *in vivo* data from GBMs suggest that YKL-40 strongly expressed by mural cells may mediate endothelial cell-based vascular coverage, stability, angiogenesis and possibly tumor malignancy.

GSCs have the ability to transdifferentiate into a large population of mural cells that stabilize blood vessels and support blood perfusion (9). To interrogate if GSCs derived from patients with GBM can recapitulate this vascular property that potentially confers radioresistance, we established xenografted tumor models in animals by transplantation of GSCs into the brains of SCID/Beige mice and following week 3 of intracranial injection, these animals were set up for a trial (six animals for each group) of a 4 week monotherapy with either anti-YKL-40 neutralizing antibody mAY (5 mg/kg, twice a week, a total of eight times) or local IR (3 Gy weekly) and a dual therapy together with mAY and IR (Figure 2A). In a total period of 9 weeks, mice receiving the single treatment with mAY or IR survived 18.4% longer (average 45.2±5.5 and 45.2±3.8 days, $n = 6$, respectively) than mIgG-treated controls (average 38.2±3.3 days, $P < 0.05$, $n = 6$). Strikingly, the dual therapy led to 42.1% longer survival (average 54.6±4.1 days) than the survival of control animals ($P < 0.01$, $n = 6$) and mAY or IR ($P < 0.05$, $n = 6$) (Figure 2A). Post-mortem examination of six tumor samples from each subset exhibited that the single therapy with either mAY or IR significantly reduced tumor growth ~60–62% compared with mIgG controls (Figure 2B and C). Consistent with the survival data, the combination therapy suppressed tumors by 81%, suggesting synergistic inhibition in tumor growth. To explore the possibility of cell death that may mediate tumor suppression treated by mAY and

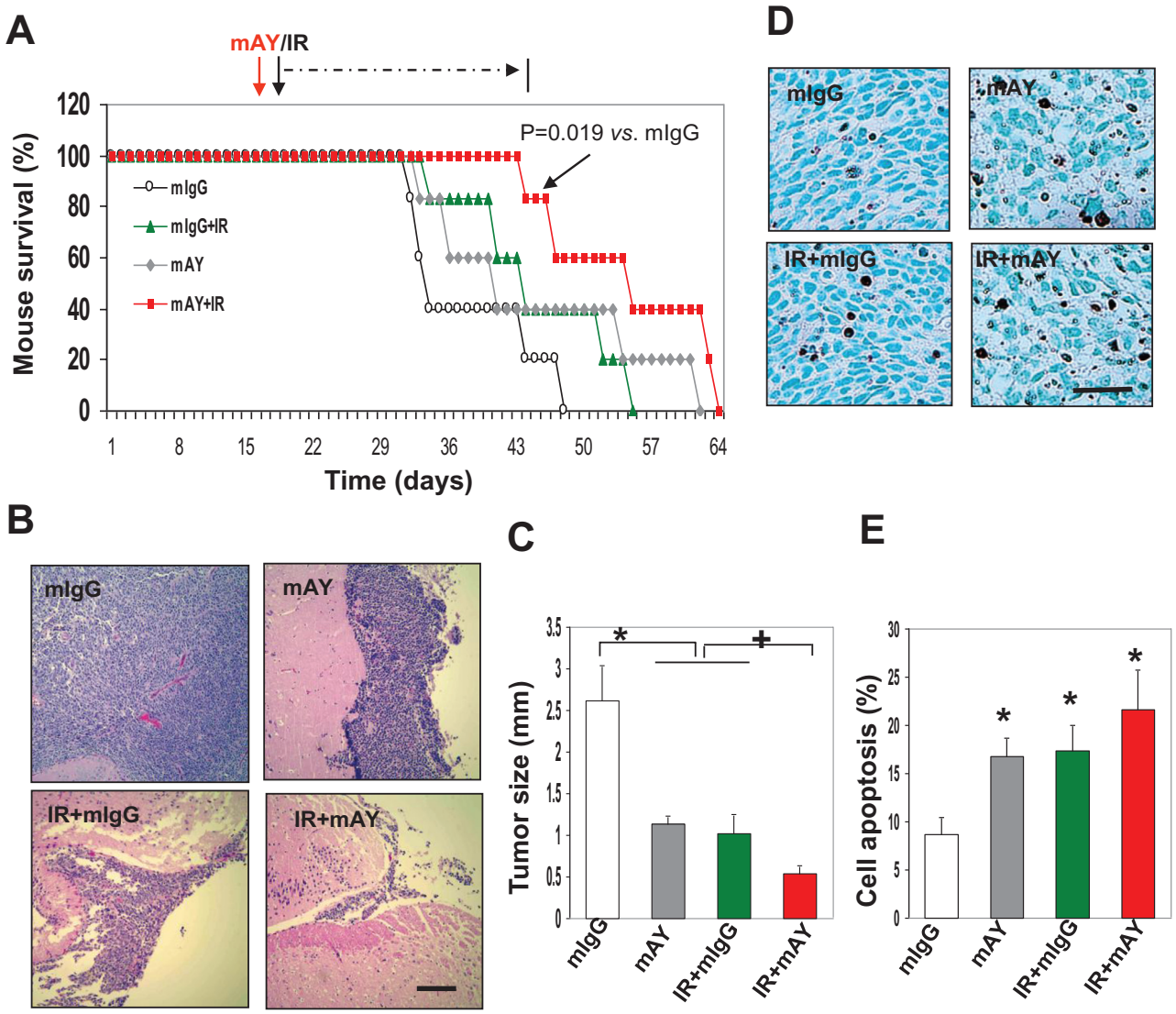

Fig. 2. mAY and IR therapy synergistically suppress tumor growth and increase mouse survival. (**A**) GSCs were injected into right striatum of SCID/Beige mice and on day 23, mice were treated with mAY, mIgG (5 mg/kg, subcutaneously twice a week), IR (3 Gy once a week) or combination for 4 weeks. Mouse survival curves were analyzed using Kaplan–Meier plot (*$P = 0.019$ compared with mIgG). $n = 6$. (**B**) Removed brains were processed in coronal sections and a fragment of the samples was used for H & E staining. Bar: 500 µm. $n = 6$. (**C**) Tumors were measured for the distance above the striatum. $n = 6$. *,+P <0.05 compared with mIgG and single IR or mAY, respectively. (**D** and **E**) Tumors were subjected to a cell apoptosis assay. Positive brown signal in nuclei was quantified from an average of six different fields in each sample. $n = 6$. *P <0.05 compared with the control. Bar: 100 µm.

IR, the tumor samples were subsequently measured for cell apoptosis (Figure 2D). mAY or IR induced cell death by 2.1-fold greater than that treated with mIgG, and the combined treatment resulted in 2.7-fold higher cell apoptosis than the controls (Figure 2E).

To further probe if mAY- or IR-inhibited tumor development also depends on the suppression of tumor neovascularization driven by GSCs, these tumor samples were analyzed for vascular markers. Blood vessels stained with an anti-CD31 antibody displayed that mAY inhibited endothelial cell vessels by 50% relative to mIgG-treated controls, whereas IR had no effect on vessels (Figure 3A and B). It was noteworthy that dual treatment with mAY and IR inhibited >90% of vessels. To characterize the reduced tumor vascularization that may be mainly ascribed to vascular dysfunction of mural cells, the samples were subjected to IHC of YKL-40 and SMa. Consistent with earlier findings in GBM, tumor vessels expressed YKL-40 and SMa, and CD31-positive vessel lumens were discernable in control and IR-treated tumors (Figure 3A). However, mAY reduced vessel expression of YKL-40 and SMa, leading to diminished vessel diameter and vessel collapse. Double treatment with mAY and IR dramatically decreased vessel lumens to 20% compared with controls (Figure 3A and B). Consistent with these results, costaining of fibrinogen and CD31 revealed that mAY, but not IR, induced vessel leakage by 2-fold greater than the control counterpart, and that the dual therapy substantially enhanced vessel leakage. All the data suggest that mAY inhibits tumor development through tumor vascular dysfunction and cell apoptosis, whereas IR induces tumor cell death but fails to impede tumor vascularization. The addition of mAY to IR leads to a synergistic inhibition in tumor vascularization and tumor cell growth, suggesting that the vascular resistance to radiotherapy may depend on expression of YKL-40 in mural cells.

In an attempt to further evaluate if mAY and IR exhibit different effects on GSC viability, we treated GSCs with mAY or IR *in vitro*. Self-renewal of GSCs was significantly blocked by mAY between days 3 and 10 by ~50–56% compared with control GSCs (Figure 4A).

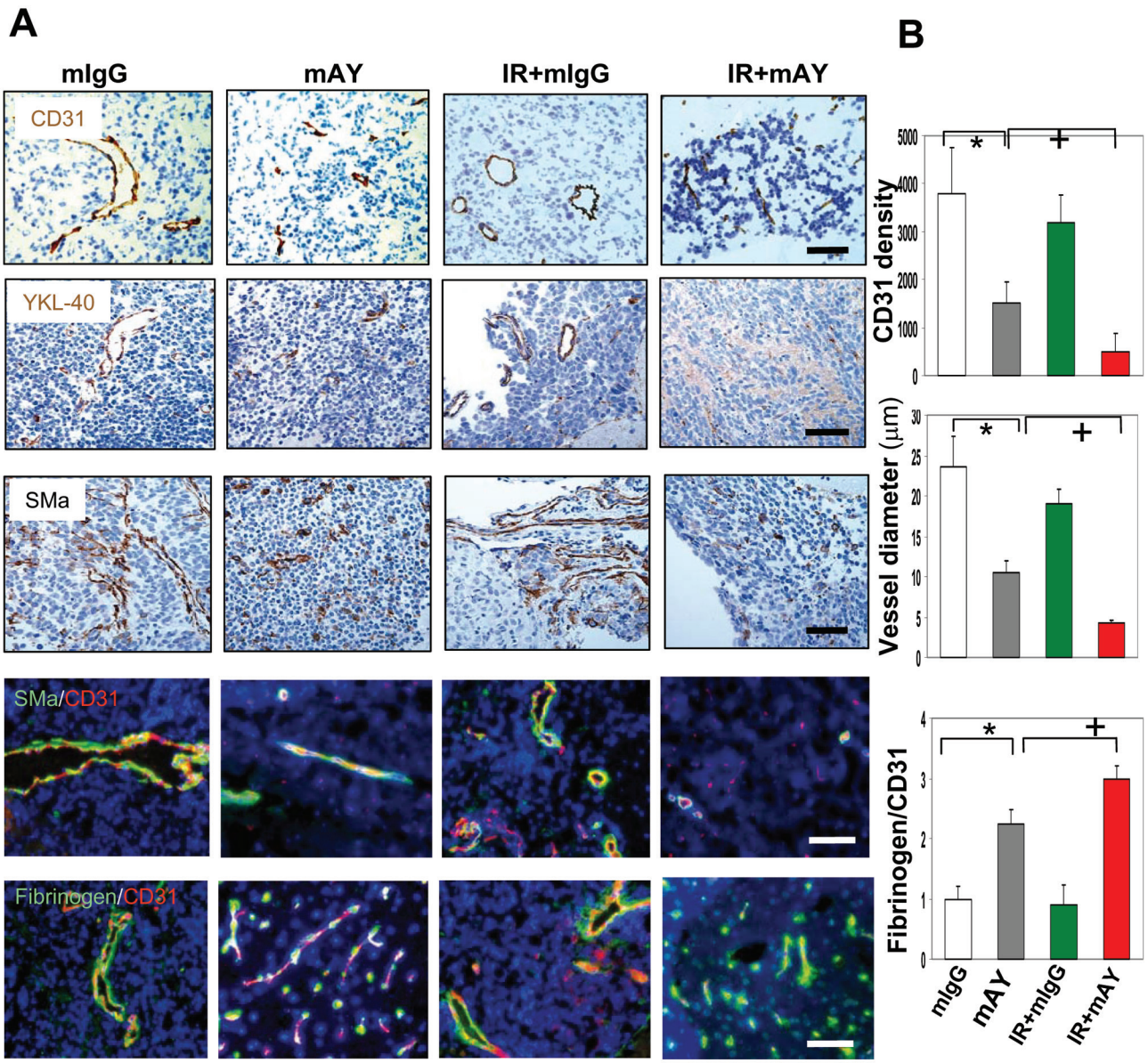

Fig. 3. mAY, but not IR, inhibits tumor angiogenesis and vessel stability, whereas IR enhances these inhibitory effects of mAY on vessels. (**A**) Animal tumor samples from Figure 2 were subjected to single staining (brown) of IHC for CD31, YKL-40 and SMa and double immunofluorescent staining for SMa (green)/CD31 (red) and fibrinogen (green)/CD31 (red). DAPI (blue) was used to stain nuclei. $n = 6$. Bars: 100 μm. (**B**) Quantification of CD31 vessel density and vessel diameter was shown from single immunohistochemical staining of CD31 in (A). Quantification of the ratio of fibrinogen versus CD31 from (A) was shown for vessel leakage. $n = 6$. $^{*,+}P < 0.05$ compared with mIgG and mAY, respectively.

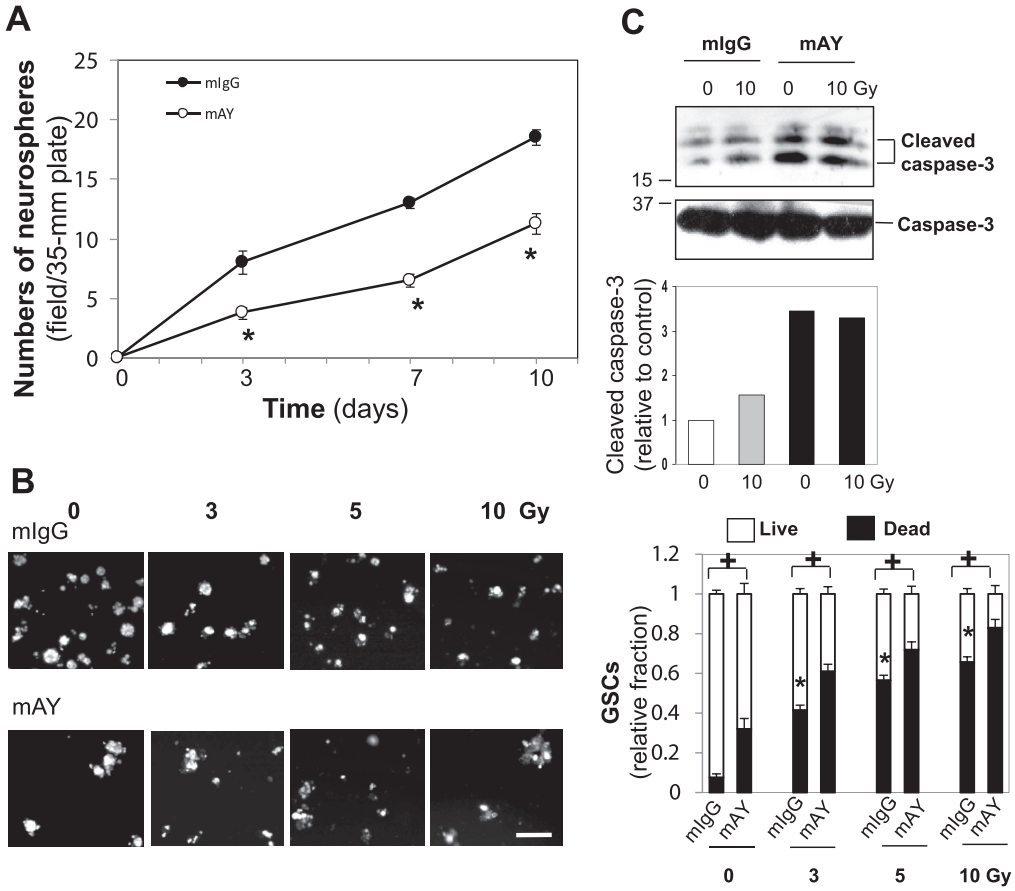

Fig. 4. mAY blocks GSC self renewal and combined treatment of mAY and IR synergistically induces GSC death. (**A**) GSCs (10^3 cells) were grown in a 35 mm plate and quantitatively analyzed for proliferation after treatment with mAY or mIgG (10 µg/ml) two times in 10 days. (**B**) Similar GSCs were also treated with IR (0–10 Gy) twice in the presence of mAY (10 µg/ml) two times in 7 days. A Live/Dead kit was used to evaluate cell viability, in which green fluorescence indicated live cells and red fluorescence was for dead cells. **P* <0.05 compared with mIgG control in the absence of IR and ^{+}P <0.05 compared with corresponding mIgG controls. *n* = 5. Bar: 50 µm. (**C**) GSCs were grown in the presence of mAY or mIgG (10 µg/ml) two times and treated with 10 Gy IR twice for 7 days. Cell lysates were used to test caspase-3 levels using immunoblotting. Density of cleaved caspase-3 bands was quantified relative to the untreated control that was set as 1 unit.

GSCs were also exposed to 3–10 Gy IR twice in 7 days in the absence or presence of mAY and then a Live/Dead kit was employed to assess cell viability (Figure 4B). Consistent with earlier findings that mAY and IR increased GSC-derived tumor cell apoptosis *in vivo* (Figure 2), mAY alone induced cell death by 2.8-fold more than did mIgG, and IR promoted cell death by 4- to 6-fold greater than the control in a dose-dependent manner (Figure 4B). Combined treatment with mAY and IR resulted in a synergistic induction in cell death. To explore molecular mechanisms underlying cell death, cell lysates from IR- and mAY-treated GSCs were analyzed for protein expression of caspase-3, an apoptosis enzyme that commits a cell death signaling cascade. A cleaved, active form of caspase-3 was elevated by IR and noticeably induced by mAY or combined treatment with IR, whereas total caspase-3 was not altered (Figure 4C), suggesting that caspase-3 may mediate the GSC apoptosis induced by IR and mAY.

In order to validate that GSC-derived mural cells possess the vascular phenotype, we isolated primary mural cells (GSC-DCs) from transdifferentiation of GSCs in 7 day culture in the presence of 10% FBS (9). The transdifferentiated mural cells are able to form vascular tubules in Matrigel culture and express genes specific for mural cells such as PDGFR, NG-2, SMa, but not CD31 or VE-cadherin (data not shown). Although IR or mAY did not significantly alter mural cell differentiation of GSCs in 7 day culture (data not shown), proliferation of GSC-DCs was reduced in the presence of IR or IR with mAY (Supplementary Figure 1, available at *Carcinogenesis* Online). To evaluate cell permeability, the same amount of GSC-DCs pretreated with mAY, IR or both were engaged in the assay that monitors cell permeability to Dextran conjugated with FITC. In a 240 min period, GSC-DC permeability was increased by treatment with mAY or mAY plus IR, whereas the permeability was not influenced by IR alone (Figure 5A). HMVEC permeability was not altered upon treatment with IR or mAY (Figure 5A), as HMVECs do not express YKL-40 (data not shown). Thus, the data suggest that the permeability of GSC-DCs and HMVECs is not altered by IR. To evaluate the overall cell permeability mediated by both GSC-DCs and HMVECs that would be more representative of vessel function *in vivo*, we loaded GSC-DCs followed by plating HMVECs on the top of the GSC-DCs, the system that simulates the vascular orientation from an "endothelial cell to mural cell" layer and encounters penetration of FITC–Dextran. Inhibition of YKL-40 with mAY increased the "vascular" permeability by 36% compared with mIgG control at 240 min (Figure 5B). Likewise, dual treatment with mAY and IR induced the permeability by 36–40% between 120 and 240 min, whereas IR did not alter the permeability. These results suggest that vascular permeability is primarily dependent on GSC-DCs and that YKL-40 blockade in GSC-DCs destabilizes the permeability.

To assess if GSC-DCs indeed act as mural cells to stabilize endothelial cell vessels, we employed a tube formation assay on Matrigel by coculturing both HMVECs and GSC-DCs. HMVECs prelabeled with Calcein AM (green fluorescence) were mixed with GSC-DCs prelabeled with Calcein Red (red fluorescence). Stability of tubules formed by HMVECs and GSC-DCs was monitored over a 24 h time course. As shown in Figure 5C, HMVECs cocultured with control GSC-DCs maintained tubules similar to those in HMVECs

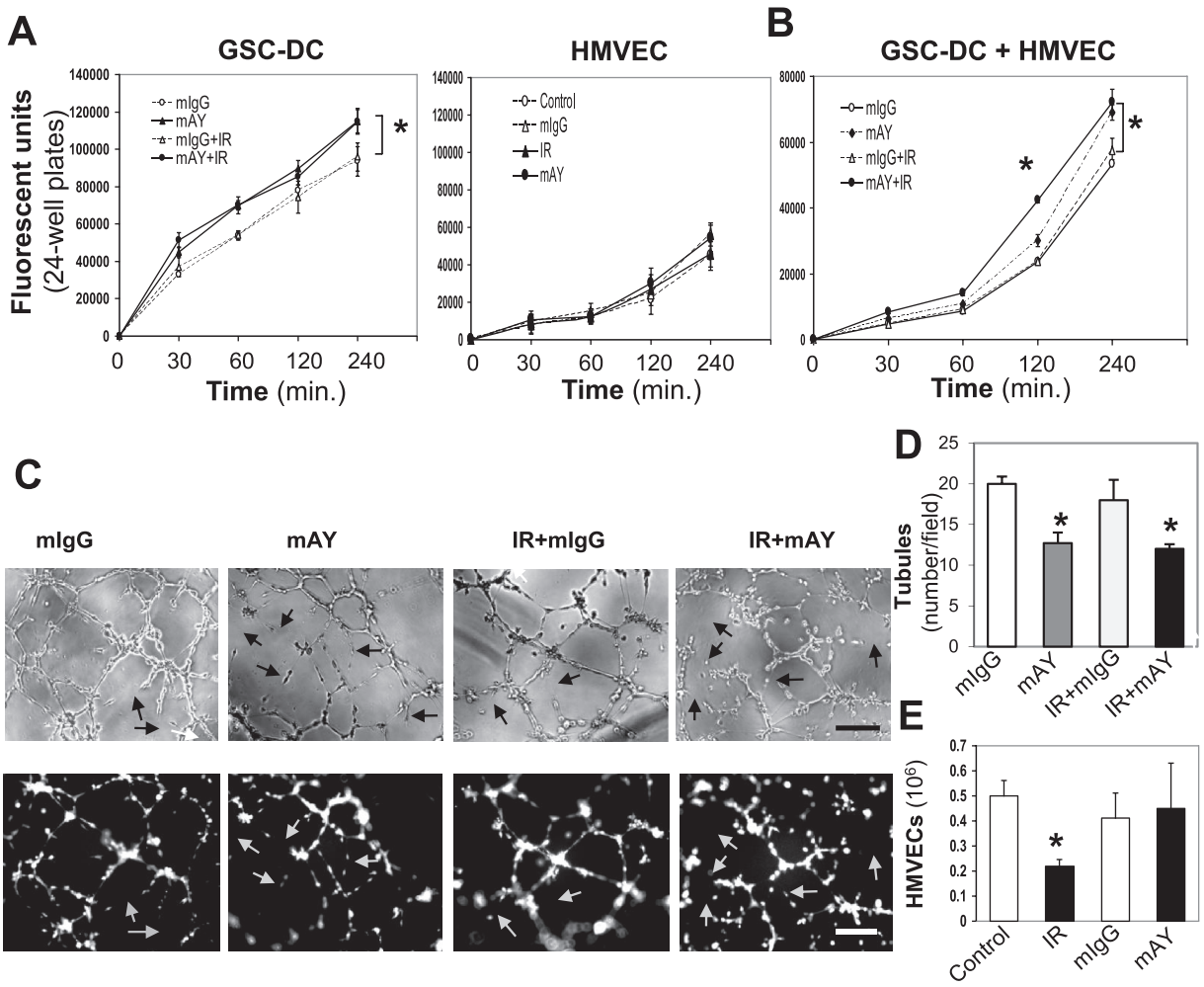

Fig. 5. mAY, but not IR, alters permeability and vessel stability of GSC-DCs. GSCs were differentiated into GSC-DCs by 10% FBS in the presence of mAY (10 μg/ml, twice), IR (10 Gy twice) or both for 7 days. (**A**) GSC-DCs were loaded onto the upper chamber of the transwell and next day, FITC-conjugated Dextran was added in the top chamber followed by measurement of fluorescence at the bottom chamber. HMVECs pretreated with mAY (10 μg/ml) or IR (10 Gy) twice for 7 days were similarly used for the cell permeability assay. $n = 4$. $^*P \leq 0.05$ compared with corresponding mIgG controls. (**B**) GSC-DCs pretreated with mAY, IR or both (twice) for 7 days were first plated on the insert. After 2 h, HMVECs were plated on the top of the GSC-DCs to form a second layer in the presence of mIgG or mAY (10 μg/ml, once). Twenty-four hours later, cell permeability assay was performed. $n = 4$, $^*P \leq 0.05$ compared with corresponding mIgG controls at the same time points. (**C**) GSC-DCs pretreated with mAY, IR or both (twice) for 7 days were labeled with Calcein Red and HMVECs were labeled with Calcein AM. Following 24 h, tubules were visualized by phase contrast and fluorescent images. (**D**) The tubules were quantified. Arrows indicate breaks in the tube networks. $^*P < 0.05$ compared with corresponding mIgG controls. $n = 3$. Bars: 200 μm. (**E**) Total number of HMVECs treated with mIgG, mAY (10 μg/ml) or 10 Gy IR twice for 7 days was quantified. $n = 3$. $^*P < 0.05$ compared with control.

cocultured with GSC-DCs pretreated with IR. In contrast, pretreatment of GSC-DCs with mAY or combination of mAY and IR led to destabilization of these tubules, as the breakdowns and gaps in the tube network, indicated by arrows, were significantly increased by 38–40% relative to mIgG-treated counterparts (Figure 5C and D). Treatment of HMVECs alone with mAY or IR did not influence tube formation or stability (data not shown), except cell proliferation reduced by IR (Figure 5E). The results, analogous with vascular permeability findings, suggest that GSC-DCs maintain the vascular ability to support and stabilize endothelial cell-lined vessels, recapitulating mural cell function found in tumors *in vivo*. In addition, the evidence that IR failed to block vascular activity in both endothelial cells and mural cells in culture, consistent with the vascular phenotype found in transplanted tumors, suggests that vascular radioresistance is dependent on vascular activity of both endothelial cells and YKL-40-expressing mural cells.

To gain insight into molecular mechanisms underlying decreased vascular stability by mAY, we investigated interaction of intercellular junction molecule N-cadherin with its intracellular associated protein β-catenin by coimmunoprecipitation followed by immunoblotting. Treatment of GSC-DCs with mAY decreased the association between N-cadherin and β-catenin, whereas IR had minimal inhibition in their interaction (Figure 6A). Combined treatment with mAY and IR inhibited their association to the extent similar to the level reduced by mAY alone. Immunocytochemistry analyses revealing their colocalization on cell membrane confirmed the inhibitory activity of mAY in the interaction between N-cadherin and β-catenin (Figure 6B). YKL-40 is known to activate membrane protein syndecan-1 through interaction with heparan sulfate chains on the ectodomain of syndecan-1 (29). To explore if YKL-40 or inhibition of YKL-40 by mAY can alter the interaction of syndecan-1 with N-cadherin, we also employed the same immunoprecipitation and immunoblotting approach and we interestingly found that mAY treatment promoted association of syndecan-1 with N-cadherin (Figure 6A), but IR or combination treatment abolished their interaction to a level lower than the basal control, despite the minimal effect of IR on N-cadherin/β-catenin association.

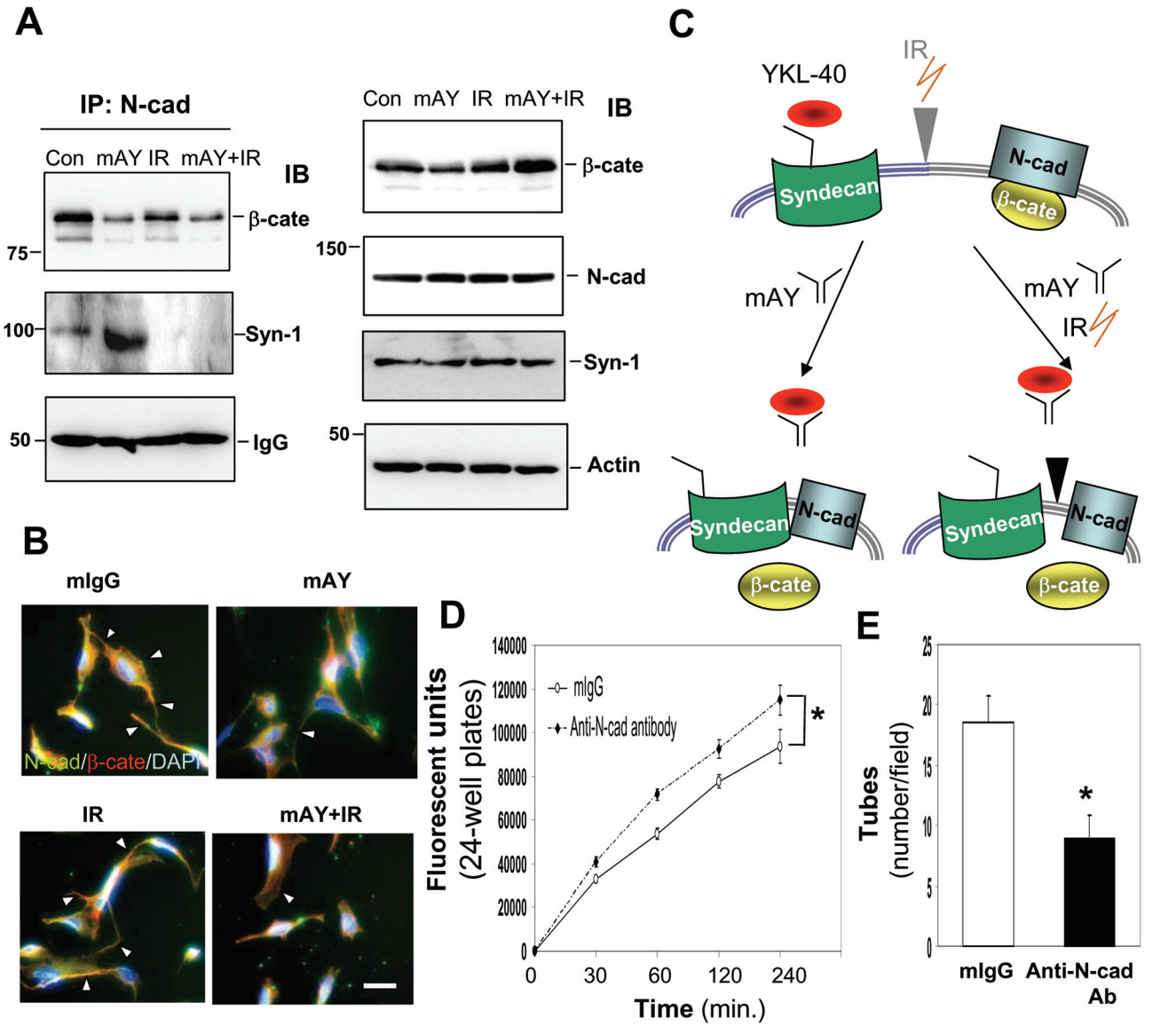

Fig. 6. N-cadherin (N-cad) plays a key role in membrane adhesion molecule interaction, vascular stability and permeability of GSC-DCs. GSCs were differentiated into GSC-DCs in the presence of IR and/or mAY twice for 7 days as described in Figure 5. (**A**) Cell lysates were used for either immunoprecipitation followed by immunoblotting or direct immunoblotting. (**B**) GSC-DCs were subjected to immunocytochemistry analysis. DAPI was stained for nuclei. Arrows indicate overlapping (yellow) of N-cad (green) and β-catenin (β-cate) (red) on cell membrane. Bar: 10 μm. (**C**) A proposed scheme for interaction of N-cad with β-cate and syndecan-1 (syn-1) in the presence of IR or mAY. (**D**) Parental GSC-DCs with no any pretreatment were exposed to a neutralizing anti-N-cad antibody (1:50; Sigma) or mIgG overnight. Then the cells were used for a permeability assay. $n = 4$, $^*P \leq 0.05$ compared with mIgG. (**E**) Parental GSC-DCs were pretreated with an anti-N-cad antibody or mIgG overnight followed by labeling with Calcein Red, and HMVECs were labeled with Calcein AM. Tube formation similar to Figure 5C was quantified. $n = 3$, *P ≤0.05 compared with mIgG.

mAY, IR or combination did not alter basal levels of N-cadherin, β-catenin or syndecan-1 except a slight decrease in β-catenin by mAY. The data suggest that blockade of YKL-40 by mAY increases the association between syndecan-1 and N-cadherin, leading to dissociation of N-cadherin from β-catenin and loss of N-cadherin membrane function (Figure 6C). Although IR does not markedly influence the interaction between N-cadherin and β-catenin, it inhibits the association of N-cadherin with syndecan-1, independent of YKL-40 activity. To further validate that N-cadherin plays a pivotal role in vascular function of GSC-DCs, a neutralizing anti-N-cadherin antibody was engaged in the permeability and stability assays (Figure 6D and E). Permeability of GSC-DCs was increased upon treatment with the anti-N-cadherin antibody compared with mIgG treatment in a 240 min period. In addition, the anti-N-cadherin antibody reduced stability of vascular tubules developed from a mixture of HMVECs and GSC-DCs by ~50% relative to control tubules. All the data suggest that intercellular N-cadherin mediates vascular activity of GSC-DCs and that mAY blocks this activity through interrupting the association of N-cadherin with β-catenin.

Discussion

Chemotherapy and radiotherapy are the most common adjuvant modality treated for patients with recurrent GBMs following primary tumor resection (1). The addition of radiotherapy to surgery increases survival of patients from a range of 3–4 months to 7–12 months (36). However, it is noteworthy that following the conventional radiotherapy with local irradiation in every week, 90% of the tumors recur at the original site (37). Chemotherapy such as a DNA synthesis inhibitor temozolomide in concomitant treatment with radiotherapy can increase the median survival to 14.6 months from 12.1 months of

patients treated with radiotherapy alone (36). Despite the encouraging evidence of either single or combined therapy, a high mortality of the disease is still static. Thus, it is urgently required to develop new efficacious drugs and also devise therapeutic strategies in the disease management. To simulate the chemotherapy and radiotherapy, the current study employed mAY and IR in an orthotopic brain tumor model in mice. The conjunction therapy with mAY and IR was found to have stronger inhibition in tumor growth and malignancy than did the single trial, underscoring an anti-YKL-40 antibody as potential intervention utility and a new combined regimen with IR for treatment of brain tumor.

In GBM patients, elevated YKL-40 was correlated with vessel stability, integrity, density and poor survival, indicating an angiogenic role of YKL-40 in tumor development and also potential mechanisms underlying tumor vascularization. Consistent with these data, mAY was identified to abrogate mural cell-mediated vascular stability and increase vascular permeability through disassociation of N-cadherin from β-catenin, thus inhibiting angiogenesis, whereas IR promoted tumor cell and endothelial cell apoptosis and it could not impair vascular activity of endothelial cells or mural cells *in vivo* and *in vitro*, highlighting tumor vascular resistance to IR. In addition to endothelial cells refractory to IR, this radioresistance is at least in part dependent on the expression of YKL-40 in mural cells, because mAY and IR synergistically inhibit angiogenesis and it is also supported by documented evidence that IR can induce YKL-40 expression in cultured tumor cells and that tumors expressing YKL-40 in patients poorly respond to IR (23,30,31). Indeed, mAY also eliminated endothelial cell angiogenesis mediated by YKL-40 as seen in xenografted tumors, consistent with our previous findings *in vitro* that mAY can diminish YKL-40-induced endothelial cell angiogenesis (35). The data support a paracrine fashion of YKL-40 derived from mural and/or tumor cells in endothelial cell vascularization *in vivo*. Therefore, this study deciphers the mechanisms by which mAY and IR coordinately suppress tumor vascularization and tumor development. Although IR was also found to prevent the association of syndecan-1 with N-cadherin, the molecular mechanisms are currently unknown. It will also be interesting to understand if this protected interaction maintains syndecan-1 function that may mediate YKL-40-induced cell adhesion. Nevertheless, the interaction between syndecan-1 and N-cadherin helps elucidate a new model for the link between YKL-40 action and N-cadherin function (Figure 6C).

In the animal models, mAY and IR combination led to synergistic suppression in tumor vascularization in xenografted tumors. However, this cooperative activity was not recapitulated in the studies *in vitro* including vascular tubule stability and permeability. This discrepancy may be ascribed to the divergent settings engaged in animals and in the cultured condition. First, IR not only promoted tumor cell death in animals but also inhibited mural cell and vascular endothelial cell proliferation *in vitro*. Thus, mAY and IR markedly inhibited tumor vessels probably through vascular cell dysfunction and impairing proliferation, respectively. In contrast, IR-inhibited vascular cell growth was not involved in our *in vitro* assays, as identical vascular cells were used. Next, we cannot rule out other possibilities that tumor-promoting factors (e.g. cytokines and chemokines) accumulated in the tumor microenvironment (38,39) may be controlled by IR, whereas these factors do not exist in the *in vitro* system.

GSCs are appreciated to possess tumor plasticity capable of differentiating into neural lineages and transdifferentiating into mural cells that mediate tumor vessel formation (9,40). To mimic this vessel-supporting activity identified in tumors *in vivo*, the primary GSC-DCs derived from GSCs were engaged following 7 day culture *in vitro*. It was noted that serum supplement in GSC culture leads to an altered genotype and/or phenotype distinct from that in the serum-free medium containing growth factors (41). Consistent with this finding, the transdifferentiated mural cells in the presence of FBS acquire mural cell gene expression such as PDGFR, NG-2, SMa, but not CD31 or VE-cadherin (data not shown). In addition, these mural cells display the vessel-supporting property as found in vascular stability and permeability *in vivo*. To minimize possibly exogenous stress in GSCs during their transdifferentiation, a 7 day short time culture in the presence of serum was used, which was sufficient to ensure the mural cell transdifferentiation and acquire vascular function that are identical to the tumor vascular phenotype characterized by transplanted GSCs in the brain where the mural cell transdifferentiation occurred (9). Therefore, GSC-DCs demonstrate a suitable system able to recapitulate the vascular signature of mural cell transdifferentiation of GSCs.

Given the low incidence of GBM in cancer patients, a larger sample pool from multiple hospitals is expected to offer solid evidence to strengthen our conclusion and firmly establish the importance of the combined regimen using mAY and IR. Interestingly, in the current small clinical trial, dual therapies with radiation and bevacizumab in GBM patients seem to be more beneficial than radiotherapy only, irrespective of YKL-40 expression. Although increased sample size is warranted to evaluate the efficacy of the combined therapy, it is noted that emerging evidence from multiple independent studies with large cohorts indicated that the overall benefits of bevacizumab treated for GBM recurrence are still controversial (42–44). In addition, it is noted that YKL-40 elevated in GBM regulates vascular endothelial growth factor expression and mediates tumor angiogenesis and radioresistance (29). Thus, the concomitant therapy with mAY, radiation and anti-vascular endothelial growth factor drugs will have benefit for patients with more aggressive GBM. Nonetheless, it should be at least taken into account that replacement of bevacizumab with an anti-YKL-40 antibody in bevacizumab-resistant patients may hold greater therapeutic promise particularly in YKL-40-expressing populations, as those patients are likely to be more responsive to YKL-40-directed treatment. Therefore, the current study not only helps establish YKL-40 expression as a prognostic marker and therapeutic target but also suggests a novel efficacious means with radiation and neutralizing YKL-40 antibody therapy against this deadly disease.

Supplementary material

Supplementary Table 1 and Figure 1 can be found at http://carcin.oxfordjournals.org/

Funding

National Institutes of Health (R01 CA120659 to R.S.).

Conflict of Interest Statement: None declared.

References

1. Wen,P.Y. *et al.* (2008) Malignant gliomas in adults. *N. Engl. J. Med.*, **359**, 492–507.
2. Norden,A.D. *et al.* (2009) Antiangiogenic therapies for high-grade glioma. *Nat. Rev. Neurol.*, **5**, 610–620.
3. Singh,S.K. *et al.* (2004) Identification of human brain tumour initiating cells. *Nature*, **432**, 396–401.
4. Zheng,H. *et al.* (2008) p53 and Pten control neural and glioma stem/progenitor cell renewal and differentiation. *Nature*, **455**, 1129–1133.
5. Beier,D. *et al.* (2007) CD133(+) and CD133(-) glioblastoma-derived cancer stem cells show differential growth characteristics and molecular profiles. *Cancer Res.*, **67**, 4010–4015.
6. Zheng,H. *et al.* (2010) PLAGL2 regulates Wnt signaling to impede differentiation in neural stem cells and gliomas. *Cancer Cell*, **17**, 497–509.
7. Kendall,S.E. *et al.* (2008) Neural stem cell targeting of glioma is dependent on phosphoinositide 3-kinase signaling. *Stem Cells*, **26**, 1575–1586.
8. Méndez,O. *et al.* (2010) Knock down of HIF-1alpha in glioma cells reduces migration *in vitro* and invasion *in vivo* and impairs their ability to form tumor spheres. *Mol. Cancer*, **9**, 133.
9. Scully,S. *et al.* (2012) Transdifferentiation of glioblastoma stem-like cells into mural cells drives vasculogenic mimicry in glioblastomas. *J. Neurosci.*, **32**, 12950–12960.
10. El Hallani,S. *et al.* (2010) A new alternative mechanism in glioblastoma vascularization: tubular vasculogenic mimicry. *Brain*, **133**(Pt 4), 973–982.
11. Ricci-Vitiani,L. *et al.* (2010) Tumour vascularization via endothelial differentiation of glioblastoma stem-like cells. *Nature*, **468**, 824–828.

12. Wang,R. *et al.* (2010) Glioblastoma stem-like cells give rise to tumour endothelium. *Nature*, **468**, 829–833.
13. Fusetti,F. *et al.* (2003) Crystal structure and carbohydrate-binding properties of the human cartilage glycoprotein-39. *J. Biol. Chem*., **278**, 37753–37760.
14. Hu,B. *et al.* (1996) Isolation and sequence of a novel human chondrocyte protein related to mammalian members of the chitinase protein family. *J. Biol. Chem*., **271**, 19415–19420.
15. Nyirkos,P. *et al.* (1990) Human synovial cells secrete a 39 kDa protein similar to a bovine mammary protein expressed during the non-lactating period. *Biochem. J*., **269**, 265–268.
16. Shackelton,L.M. *et al.* (1995) Identification of a 38-kDa heparin-binding glycoprotein (gp38k) in differentiating vascular smooth muscle cells as a member of a group of proteins associated with tissue remodeling. *J. Biol. Chem*., **270**, 13076–13083.
17. Rehli,M. *et al.* (1997) Molecular characterization of the gene for human cartilage gp-39 (CHI3L1), a member of the chitinase protein family and marker for late stages of macrophage differentiation. *Genomics*, **43**, 221–225.
18. Kzhyshkowska,J. *et al.* (2007) Human chitinases and chitinase-like proteins as indicators for inflammation and cancer. *Biomark. Insights*, **2**, 128–146.
19. Malinda,K.M. *et al.* (1999) Gp38k, a protein synthesized by vascular smooth muscle cells, stimulates directional migration of human umbilical vein endothelial cells. *Exp. Cell Res*., **250**, 168–173.
20. Scully,S. *et al.* (2011) Inhibitory activity of YKL-40 in mammary epithelial cell differentiation and polarization induced by lactogenic hormones: a role in mammary tissue involution. *PLoS One*, **6**, e25819.
21. Nigro,J.M. *et al.* (2005) Integrated array-comparative genomic hybridization and expression array profiles identify clinically relevant molecular subtypes of glioblastoma. *Cancer Res*., **65**, 1678–1686.
22. Tanwar,M.K. *et al.* (2002) Gene expression microarray analysis reveals YKL-40 to be a potential serum marker for malignant character in human glioma. *Cancer Res*., **62**, 4364–4368.
23. Pelloski,C.E. *et al.* (2005) YKL-40 expression is associated with poorer response to radiation and shorter overall survival in glioblastoma. *Clin. Cancer Res*., **11**, 3326–3334.
24. Nutt,C.L. *et al.* (2005) YKL-40 is a differential diagnostic marker for histologic subtypes of high-grade gliomas. *Clin. Cancer Res*., **11**, 2258–2264.
25. Hormigo,A. *et al.* (2006) YKL-40 and matrix metalloproteinase-9 as potential serum biomarkers for patients with high-grade gliomas. *Clin. Cancer Res*., **12**, 5698–5704.
26. Ku,B.M. *et al.* (2011) CHI3L1 (YKL-40) is expressed in human gliomas and regulates the invasion, growth and survival of glioma cells. *Int. J. Cancer*, **128**, 1316–1326.
27. Saidi,A. *et al.* (2008) Experimental anti-angiogenesis causes upregulation of genes associated with poor survival in glioblastoma. *Int. J. Cancer*, **122**, 2187–2198.
28. Shao,R. (2013) YKL-40 acts as an angiogenic factor to promote tumor angiogenesis. *Front. Physiol*., **4**, 122.
29. Shao,R. *et al.* (2009) YKL-40, a secreted glycoprotein, promotes tumor angiogenesis. *Oncogene*, **28**, 4456–4468.
30. Francescone,R.A. *et al.* (2011) Role of YKL-40 in the angiogenesis, radioresistance, and progression of glioblastoma. *J. Biol. Chem*., **286**, 15332–15343.
31. Junker,N. *et al.* (2005) Regulation of YKL-40 expression during genotoxic or microenvironmental stress in human glioblastoma cells. *Cancer Sci*., **96**, 183–190.
32. Carmeliet,P. *et al.* (2011) Molecular mechanisms and clinical applications of angiogenesis. *Nature*, **473**, 298–307.
33. Hellström,M. *et al.* (2001) Lack of pericytes leads to endothelial hyperplasia and abnormal vascular morphogenesis. *J. Cell Biol*., **153**, 543–553.
34. Francescone,R. *et al.* (2013) Tumor-derived mural-like cells coordinate with endothelial cells: role of YKL-40 in mural cell-mediated angiogenesis. *Oncogene*, in press.
35. Faibish,M. *et al.* (2011) A YKL-40-neutralizing antibody blocks tumor angiogenesis and progression: a potential therapeutic agent in cancers. *Mol. Cancer Ther*., **10**, 742–751.
36. Stupp,R. *et al.*; European Organisation for Research and Treatment of Cancer Brain Tumor and Radiotherapy Groups; National Cancer Institute of Canada Clinical Trials Group. (2005) Radiotherapy plus concomitant and adjuvant temozolomide for glioblastoma. *N. Engl. J. Med*., **352**, 987–996.
37. Hochberg,F.H. *et al.* (1980) Assumptions in the radiotherapy of glioblastoma. *Neurology*, **30**, 907–911.
38. Leung,S.Y. *et al.* (1997) Monocyte chemoattractant protein-1 expression and macrophage infiltration in gliomas. *Acta Neuropathol*., **93**, 518–527.
39. Samaras,V. *et al.* (2007) Application of the ELISPOT method for comparative analysis of interleukin (IL)-6 and IL-10 secretion in peripheral blood of patients with astroglial tumors. *Mol. Cell. Biochem*., **304**, 343–351.
40. Cheng,L. *et al.* (2013) Glioblastoma stem cells generate vascular pericytes to support vessel function and tumor growth. *Cell*, **153**, 139–152.
41. Lee,J. *et al.* (2006) Tumor stem cells derived from glioblastomas cultured in bFGF and EGF more closely mirror the phenotype and genotype of primary tumors than do serum-cultured cell lines. *Cancer Cell*, **9**, 391–403.
42. Verhoeff,J.J. *et al.* (2009) Concerns about anti-angiogenic treatment in patients with glioblastoma multiforme. *BMC Cancer*, **9**, 444.
43. Rinne,M.L. *et al.* (2013) Update on bevacizumab and other angiogenesis inhibitors for brain cancer. *Expert Opin. Emerg. Drugs*, **18**, 137–153.
44. Wick,W. *et al.* (2010) Bevacizumab and recurrent malignant gliomas: a European perspective. *J. Clin. Oncol*., **28**, e188–9; author reply e190.

Received July, 10, 2013; revised November 14, 2013; accepted November 19, 2013